J. Fluid Mech. (1981), *vol.* 108, *pp.* 247–272
Printed in Great Britain

Convection in an imposed magnetic field. Part 1. The development of nonlinear convection

By N. O. WEISS

Department of Applied Mathematics and Theoretical Physics, University of Cambridge

(Received 25 June 1980)

Nonlinear two-dimensional magnetoconvection in a Boussinesq fluid has been studied in a series of numerical experiments with values of the Chandrasekhar number $Q \leqslant 4000$ and the ratio ζ of the magnetic to the thermal diffusivity in the range $1 \geqslant \zeta \geqslant 0{\cdot}025$. If the imposed field is strong enough, convection sets in as overstable oscillations which give way to steady convection as the Rayleigh number R is increased. In the dynamical regime that follows, magnetic flux is concentrated into sheets at the sides of the cells, from which the motion is excluded.

1. Introduction

The interaction between magnetic fields and convection can be observed directly in the Sun. Where the field is strong, as in sunspots, normal convection is inhibited. Where the average field strength is less, magnetic flux is concentrated into isolated tubes or ropes, and such intermittent structures seem to be characteristic of turbulent magnetic fields. These situations cannot be modelled in the laboratory. Numerical experiments are, however, possible and the aim of this pair of papers is to explore the nonlinear, dynamical interaction between magnetic fields and convection.

In order to investigate the effect of the Lorentz force on convection we must solve the equation of motion, together with the induction equations, for a particular configuration. The natural model problem is that of convection in a Boussinesq fluid heated from below in the presence of an imposed vertical magnetic field. It is convenient to adopt the simplest consistent set of boundary conditions, so that the normal velocity and the tangential components of both the viscous and the magnetic stress vanish at the top and bottom of the convecting layer. Previous work has often been reviewed (Cowling 1957; Chandrasekhar 1961; Roberts 1967; Spiegel 1972; Weiss 1977). These two papers present the results of an extensive series of numerical experiments on two-dimensional magnetoconvection. Part 1 is concerned with the onset of steady, finite-amplitude convection and the transition from oscillatory to steady motion. Part 2 covers the whole dynamical regime, including the transition to kinematic behaviour when the field is relatively weak.

The simpler kinematic problem, where the field is feeble enough for the Lorentz force to be neglected, is now well understood. When the magnetic Reynolds number is large, flux is eventually expelled from the convective eddies and concentrated into isolated tubes between them. Solutions have been obtained for various choices of velocity (Parker 1963, 1979; Clark 1965, 1966; Weiss 1966; Clark & Johnson 1967; Busse 1975; Galloway & Weiss 1981). In all these examples, the transverse component

of the velocity vanishes at the centre of the tube and varies linearly across it; flux concentration is limited by diffusion and the field has a Gaussian profile (e.g. Proctor & Weiss 1978).

The full dynamical problem can only be understood by reference to linear theory. The static, conducting solution loses stability when the Rayleigh number R exceeds a critical value. The form of this bifurcation depends on the ratio of the magnetic diffusivity η to the thermal diffusivity κ. If $\eta > \kappa$, the eigenvalues are real and convection sets in as a direct (or monotonic) instability at $R = R^{(e)}$; if $\eta < \kappa$ (the astrophysically interesting case) convection may first appear as an oscillatory (or overstable) mode corresponding to a Hopf bifurcation at $R = R^{(o)}$ (Thompson 1951; Chandrasekhar 1952, 1961; Danielson 1961; Weiss 1964).

Nonlinear theory is of course more difficult. Veronis (1959) used modified perturbation theory to obtain finite-amplitude solutions in the neighbourhood of $R^{(e)}$, and mildly nonlinear oscillations can be followed when $R^{(o)}$ is almost equal to $R^{(e)}$ (Knobloch & Proctor 1981). Busse (1975) expanded about R_0, the critical Rayleigh number in the absence of a magnetic field, and demonstrated the possibility of subcritical steady convection, with $R < R^{(e)}$, for $\eta < \kappa$. Here we provide the first systematic study of the development of nonlinear magnetoconvection. A preliminary account of some of these results was given by Weiss (1975) and Spiegel (1972) reports similar calculations by J. Wright. Analogous solutions for axisymmetric magnetoconvection in a cylindrical container have been published by Galloway & Moore (1979).

For $\eta < \kappa$ the calculations presented here do indeed show, as R is increased, the development of nonlinear oscillations followed by the appearance of steady convection. Subcritical steady solutions, with $R < R^{(e)}$, are possible because the magnetic flux is confined to sheets on either side of a convection cell, so facilitating motion in the field-free central region. When the imposed magnetic field, B_0, is sufficiently weak the field profile in these sheets is approximately Gaussian and the values of $R_{\min}$, the lowest value of R for which steady motion can occur, agree with Busse's (1975) predictions.

If B_0 is larger an entirely new regime is found. The flux sheets become dynamically active and the magnetic field generates vorticity with the opposite sense to that in the convective eddy until motion is excluded from the flux sheets (Peckover & Weiss 1978; Galloway, Proctor & Weiss 1978). The horizontal component of the velocity no longer varies linearly across the flux sheets, which are virtually stagnant. Within them the field is nearly uniform, dropping abruptly in narrow current sheets at the interfaces between flux sheets and adjacent eddies. The field profile, which has a shape like a cocked hat for kinematic concentration, looks more like a top-hat in this regime. For B_0 sufficiently large and $\eta/\kappa \lesssim 0{\cdot}2$ steady convection first appears with the flux concentrated into sheets from which the motion is excluded. Moreover, the value of $R_{\min}$ and the field strength in the flux sheet are found to be independent of η when $\eta/\kappa \ll 1$; from the numerical experiments it seems that steady convection first appears when the reduced free-fall velocity is roughly equal to the Alfvén speed, so that the temperature difference across the layer is proportional to B_0^2 but does not depend on any of the diffusivities.

When $R^{(o)} < R_{\min} < R^{(e)}$ there is a range $R_{\min} < R < R_{\max}$ in which both oscillatory and steady solutions are possible. The transition from large-amplitude oscillations to steady convection is fascinating but rather mystifying. Fortunately, it is possible to construct a simple fifth-order system of ordinary differential equations whose solutions

mimic those of the full two-dimensional problem (Knobloch, Weiss & Da Costa 1981). This fifth-order model has been studied in detail and is a reliable guide both to the bifurcation structure of the full problem and to the nature of the transition from oscillatory to steady motion at $R = R_{\max}$. In general, the oscillations increase in period as R approaches $R_{\max}$. For certain values of the parameters the period becomes infinite at $R_{\max}$: thus the branch of oscillatory solutions terminates on an (unstable) position of the steady branch. For other values there is a bifurcation from oscillations that are symmetrical about the static state to asymmetrical oscillations, with a preference for one or the other sense of motion (depending on the initial conditions). It remains unclear whether this is ever followed by a further sequence of bifurcations leading to aperiodic oscillations before the oscillations lose stability to the steady branch.

The two-dimensional problem is defined in the next section. This is followed by summaries of linear theory and finite-amplitude expansions, without which the nonlinear results would be incomprehensible. The results of numerical experiments with comparatively low values of B_0 are contained in § 4, while runs in which motion is excluded from the flux sheets are described in § 5. Nonlinear oscillations and the transition to steady motion are discussed in § 6, which is followed by a description of the onset of steady subcritical convection at $R = R_{\min}$. The final section summarizes the most important results and relates them to other examples of double diffusive convection.

2. The model problem

In a Boussinesq fluid with velocity $\mathbf{u}$, the temperature T and the magnetic field $\mathbf{B}$ satisfy the equations

$$\frac{\partial T}{\partial t} = -\nabla.(T\mathbf{u}) + \kappa\nabla^2 T, \tag{2.1}$$

$$\frac{\partial \mathbf{B}}{\partial t} = \nabla \wedge (\mathbf{u} \wedge \mathbf{B}) + \eta\nabla^2\mathbf{B}, \tag{2.2}$$

with

$$\nabla.\mathbf{u} = 0 \quad \text{and} \quad \nabla.\mathbf{B} = 0. \tag{2.3}$$

The equation governing the vorticity $\boldsymbol{\omega} = \nabla \wedge \mathbf{u}$, formed by taking the curl of the equation of motion, is

$$\frac{\partial \boldsymbol{\omega}}{\partial t} = \nabla \wedge (\mathbf{u} \wedge \boldsymbol{\omega}) + \rho_0^{-1}\nabla \wedge (\mathbf{j} \wedge \mathbf{B}) - \alpha\nabla T \wedge \mathbf{g} + \nu\nabla^2\boldsymbol{\omega}, \tag{2.4}$$

where the electric current $\mathbf{j} = \mu^{-1}\nabla \wedge \mathbf{B}$ and the density $\rho = \rho_0[1 - \alpha(T - T_0)]$; $\mathbf{g}$ is the gravitational acceleration, α is the coefficient of thermal expansion and ρ_0 is the density at the reference temperature T_0.

We shall consider two-dimensional convection in a layer confined between fixed horizontal planes, referred to Cartesian co-ordinates with the z axis pointing vertically upwards. Both the velocity and the magnetic field are restricted to the xz plane and independent of y. Let $\mathbf{e}_y$ be a unit vector in the y direction; then the vector potential

$\mathbf{A} = A\mathbf{e}_y$, and $\mathbf{B}$ and $\mathbf{u}$ are described by a flux function $A(x,z)$ and a stream function $\psi(x,z)$ such that

$$\mathbf{B} = \left(-\frac{\partial A}{\partial z}, 0, \frac{\partial A}{\partial x}\right), \quad \mathbf{u} = \left(-\frac{\partial \psi}{\partial z}, 0, \frac{\partial \psi}{\partial x}\right), \tag{2.5}$$

while

$$\mathbf{j} = j\mathbf{e}_y = -\mu^{-1}\nabla^2 A\mathbf{e}_y, \quad \boldsymbol{\omega} = \omega\mathbf{e}_y = -\nabla^2\psi\mathbf{e}_y. \tag{2.6}$$

Then equation (2.2) can be integrated to give

$$\frac{\partial A}{\partial t} = -\nabla.(A\mathbf{u}) + \eta\nabla^2 A \tag{2.7}$$

and (2.4) becomes

$$\frac{\partial \omega}{\partial t} = -\nabla.(\omega\mathbf{u}) + \rho_0^{-1}\nabla.(j\mathbf{B}) - g\alpha\frac{\partial T}{\partial x} + \nu\nabla^2\omega. \tag{2.8}$$

A particular configuration is specified by five dimensionless parameters. For convection in the region $\{0 < x < \lambda d;\ 0 < z < d\}$ driven by a vertical temperature difference ΔT, in the presence of a horizontally averaged field that is vertical with magnitude B_0, these are the Rayleigh number

$$R = \frac{g\alpha\,\Delta T\,d^3}{\kappa\nu}, \tag{2.9}$$

the square of the Hartmann number (or Chandrasekhar number)

$$Q = \frac{B_0^2 d^2}{\mu\rho_0\eta\nu}, \tag{2.10}$$

the Prandtl numbers

$$\sigma = \nu/\kappa \quad \text{and} \quad \zeta = \eta/\kappa \tag{2.11}$$

and the normalized cell width λ. To reduce the number of parameters, all the nonlinear computations that will be described in this paper have $\sigma = 1$ and $\lambda = 1$ (corresponding to square cells).

It is convenient to measure lengths in terms of the layer depth d, time in terms of the thermal timescale d^2/κ, temperature in terms of ΔT and magnetic fields in terms of the imposed field B_0. From henceforth all quantities will be expressed in dimensionless form unless specifically stated otherwise. Then (2.1), (2.7) and (2.8) become

$$\frac{\partial T}{\partial t} = -\nabla.(T\mathbf{u}) + \nabla^2 T, \tag{2.12}$$

$$\frac{\partial A}{\partial t} = -\nabla.(A\mathbf{u}) + \zeta\nabla^2 A \tag{2.13}$$

and

$$\frac{\partial \omega}{\partial t} = -\nabla.(\omega\mathbf{u}) + \sigma\left[\zeta Q\nabla.(j\mathbf{B}) - R\frac{\partial T}{\partial x} + \nabla^2\omega\right], \tag{2.14}$$

where the dimensionless current $j = -\nabla^2 A$. Equations (2.12)–(2.14) must be solved together with

$$\nabla^2\psi = -\omega \tag{2.15}$$

in the region $\{0 < x < \lambda;\ 0 < z < 1\}$ subject to appropriate boundary conditions.

The simplest boundary conditions are the extension to magnetohydrodynamics of the 'free' boundary conditions used for ordinary Rayleigh–Bénard convection

(Chandrasekhar 1961). We assume that the temperature is fixed at the upper and lower boundaries and that there is no lateral heat flux, that the total magnetic flux through the region remains constant, and that the normal velocity, together with the tangential components of both the viscous and magnetic stresses, vanishes on all the boundaries. Thus

$$T = 1 \quad (z = 0), \quad T = 0 \quad (z = 1), \quad \partial T/\partial x = 0 \quad (x = 0, \lambda), \tag{2.16}$$

$$A = 0 \quad (x = 0), \quad A = \lambda \quad (x = \lambda), \quad \partial A/\partial z = 0 \quad (z = 0, 1) \tag{2.17}$$

and

$$\psi = \omega = 0 \quad (x = 0, \lambda; \quad z = 0, 1). \tag{2.18}$$

These boundary conditions do not correspond to any physically realizable configuration. Stress-free boundaries are, however, more plausible in astrophysical than in laboratory applications. The lines of force are not fixed and can move laterally at $z = 0,1$ but, from (2.17), B_x vanishes on all the boundaries. These boundary conditions give solutions that are periodic in both x and z, with sines and cosines as eigenfunctions of the linear problem (Chandrasekhar 1961). Gibson (1966) showed that the criteria for the onset of instability were not substantially altered when more realistic boundary conditions were adopted.

The system just defined is highly nonlinear and in general the equations must be solved numerically on a computer. The results in this paper were obtained using the methods described by Moore, Peckover & Weiss (1973). The parabolic equations (2.12)–(2.14) were integrated using a centred second-order finite-difference method on a staggered mesh, with a leap-frog scheme for the nonlinear terms combined with the Dufort–Frankel scheme for the diffusive terms. The Poisson equation (2.15) was solved by Fourier analysis in the x direction combined with tridiagonal elimination in the z direction. The mesh used had equal intervals in each direction; the number of intervals in the x direction, N_x, was fixed at 12, 24, or 48 and the number of intervals in the z direction, $N_z = N_x/\lambda$. Accuracy has been discussed elsewhere (Moore *et al.* 1973; Moore & Weiss 1973). The computer code is closely related to others used to study Rayleigh–Bénard convection (Moore & Weiss 1973), magnetic Oberbeck convection (Peckover & Weiss 1978) and double-diffusive convection (Huppert & Moore 1976). The numerical procedures were checked by comparing critical Rayleigh numbers, growth rates and periods for small perturbations with those predicted by linear theory. The computational results also agree well with the finite-amplitude theory developed in the next section.

3. Small-amplitude convection

3.1. *Linear theory*

Nonlinear convection cannot be understood without reference to the growth of small disturbances. The simplest case is that of a perfect fluid with all diffusivities equal to zero (Walén 1949; Cowling 1953, 1957). The unstable thermal stratification tends to produce convection, while the magnetic field supports oscillations which correspond to trapped hydromagnetic waves. Consider small perturbations that vary as e^{st} and let

$$b^2 = 1 + 1/\lambda^2. \tag{3.1}$$

Then, in dimensional terms,

$$s^2 = \frac{(b^2-1)}{b^2}\frac{g\alpha\,\Delta T}{d} - \frac{\pi^2 B_0^2}{\mu\rho_0 d^2}; \tag{3.2}$$

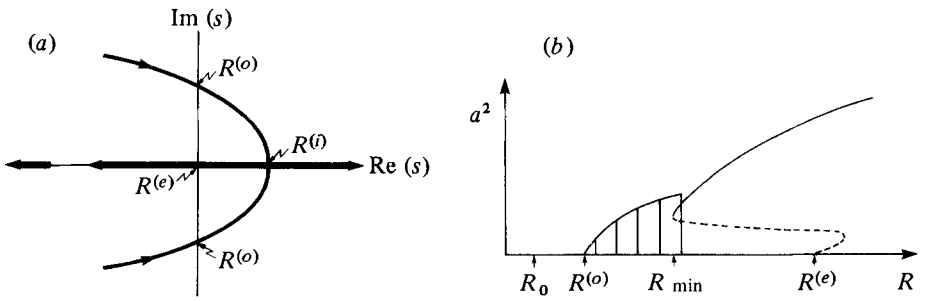

FIGURE 1. (*a*) Eigenvalues of the linear problem: behaviour of eigenvalues in the complex-s plane as the Rayleigh number is increased, when convection sets in as overstable oscillations. (*b*) The nonlinear regime: sketch showing the branch of oscillatory solutions bifurcating from $R^{(o)}$ and the branch of steady solutions bifurcating from $R^{(e)}$. Stable steady solutions exist for $R > R_{\min}$, where $R^{(o)} < R_{\min} < R^{(e)}$.

s^2 is real and the system is unstable if the magnetic term is smaller than the buoyancy term. It follows from (3.2) that as ΔT is increased for fixed B_0 instability sets in with elongated cells ($b^2 \gg 1$) when $g\alpha\,\Delta T = \pi^2 B_0^2/\mu\rho_0 d$, though square cells ($b^2 = 2$) become unstable when ΔT has been doubled.

The problem is more interesting when the diffusivities are finite (Thompson 1951; Chandrasekhar 1952, 1961; Danielson 1961; Weiss 1964). The eigenvalue s satisfies a cubic characteristic equation and there is a marginal state ($s = 0$) when $R = R^{(e)}$, where

$$R^{(e)} = R_0 + \pi^2 \frac{b^2}{(b^2-1)} Q \tag{3.3}$$

and

$$R_0 = \pi^4 \frac{b^6}{(b^2-1)}, \tag{3.4}$$

is the value of $R^{(e)}$ in the absence of a magnetic field. For $\zeta > 1$ the only bifurcation from the static solution occurs at $R = R^{(e)}$ and the system is unstable for $R > R^{(e)}$. If $\zeta < 1$ and

$$Q > Q_0 = \pi^2 b^4 \zeta(1+\sigma)/[\sigma(1-\zeta)], \tag{3.5}$$

convection sets in as an oscillatory or overstable mode. The behaviour of the eigenvalue s is sketched in figure 1 (*a*) (cf. Weiss 1964). Of the three solutions to the characteristic equation, one is always real and negative (corresponding to a stable solution). For $R < R^{(o)}$ the other two eigenvalues are complex conjugates with negative real parts. When $R = R^{(o)}$ these eigenvalues are pure imaginary; as R increases, they have positive real parts but their imaginary parts decrease until $R = R^{(i)}$, when there are two equal real eigenvalues. For $R > R^{(i)}$ both eigenvalues are real: one increases monotonically with R, the other decreases and passes through zero when $R = R^{(e)}$ (which therefore corresponds to a transition from instability to stability for that solution).

The onset of overstability occurs when $R = R^{(o)}$, where

$$R^{(o)} = \pi^2 \frac{b^2}{(b^2-1)} \frac{(\sigma+\zeta)(1+\zeta)}{\sigma} \left[\pi^2 b^4 + \frac{\sigma\zeta}{(1+\sigma)(1+\zeta)} Q\right]. \tag{3.6}$$

In a star the radiative conductivity is normally large and $Q \gg \zeta^{-1} \gg 1$; from (3.6)

$$R^{(o)} \approx \pi^2 \frac{b^2}{(b^2-1)} \frac{\sigma}{(1+\sigma)} \zeta Q \tag{3.7}$$

if $Q/b^4 \gg \zeta^{-1} \gg 1$. The transition from oscillatory to direct (or monotonic) modes occurs when $R = R^{(i)}$. To evaluate $R^{(i)}$ it is necessary to solve the cubic given in equations (159)–(163) of Weiss (1964). For all calculations in this paper $\sigma = 1$ and the cubic then simplifies to

$$(r-1)^3 - q[2r^2 + (\zeta - q)\, r - \tfrac{1}{4}] = 0, \tag{3.8}$$

where

$$q = \frac{\pi^2 b^4 (1-\zeta)^2}{\zeta Q} \quad \text{and} \quad r = \frac{(b^2-1)\, R}{\pi^2 b^2 \zeta Q}. \tag{3.9}$$

When $\zeta \ll 1$ and $(\zeta Q/b^4)^{\frac{1}{3}} \gg 1$

$$R^{(i)} \approx \pi^2 \frac{b^2}{(b^2-1)} \zeta Q; \tag{3.10}$$

in fact this result holds for all σ and $\zeta < 1$ provided that Q is sufficiently large. Now ζQ, like R, has the product $\kappa\nu$ in the denominator and does not depend on η. In this limit, therefore, the transition to direct modes corresponds exactly to the instability criterion derived from (3.2), in which no diffusivities appear. The finite thermal diffusivity does, however, allow overstability for $R < R^{(i)}$.

3.2. *Modified perturbation theory*

Near $R = R^{(e)}$ steady finite-amplitude solutions can be obtained using the expansion procedure devised by Malkus & Veronis (1958), which was first applied to magneto-convection by Veronis (1959, in a footnote). If all quantities are expanded in terms of a small parameter a such that

$$\psi = a \sin(\pi x/\lambda) \sin \pi z + O(a^3), \quad R = R^{(e)} + a^2 R_2 + O(a^3), \tag{3.11}$$

then

$$R_2 = \frac{\pi^2}{8}\left[\pi^2 b^4 + Q\left\{1 + \frac{2\lambda^2(1-\lambda^2)}{(\lambda^2+1)\,\zeta^2}\right\}\right]. \tag{3.12}$$

In general R_2 may be either positive or negative, depending on the values of λ and ζ, but if $\lambda \leqslant 1$ then $R_2 > 0$ for all ζ. Thus there exist steady finite-amplitude solutions with R just greater than $R^{(e)}$.

The stability of these solutions is discussed in detail by Knobloch *et al.* (1981). If $\zeta \geqslant 1$ or $Q < Q_0$, defined in (3.5), there are no overstable solutions. For $R_2 > 0$ the simple bifurcation at $R = R^{(e)}$ is supercritical and the finite-amplitude solutions are stable near the onset of convection. If $\zeta < 1$ and $Q > Q_0$ there is a Hopf bifurcation at $R = R^{(o)}$, which is supercritical for $\lambda = 1$. When overstability sets in first the steady solutions are always unstable in the neighbourhood of the bifurcation at $R = R^{(e)}$, regardless of the sign of R_2.

3.3. *Gaussian flux tubes*

When $\zeta \ll 1$ the above expansion can be extended into the regime where the Péclet number is still small but the magnetic Reynolds number $R_m = a/\zeta$ is large. Suppose that $\lambda = 1$ and

$$\psi = a \sin \pi x \sin \pi z. \tag{3.13}$$

Then we can consider the simplified kinematic problem and solve (2.13) and (2.17) for the magnetic field (Busse 1975; Galloway & Weiss 1981). When $R_m \gg 1$ nearly all the flux is eventually expelled from the eddy and concentrated into narrow sheets (or tubes) at $x = 0, 1$. The width ϵ of these sheets can easily be estimated (e.g. Proctor & Weiss 1978). Near the stagnation point at $x = z = 0$, $\psi \approx \pi^2 axz$ so that the horizontal component of the velocity $u \approx -\pi^2 ax$. The induction equation is satisfied by a vertical field, $\mathbf{B} = (0, 0, B(x))$, confined to a sheet with half-width ϵ such that

$$B(x) = B^* \exp(-x^2/\epsilon^2), \quad \epsilon = (\sqrt{2}/\pi) R_m^{-\frac{1}{2}}. \tag{3.14}$$

Flux conservation then requires that the peak field

$$B^* = \sqrt{(2\pi)} R_m^{\frac{1}{2}}. \tag{3.15}$$

In this kinematic solution u varies linearly with x near the edge of the cell and the field has a Gaussian profile, while $\epsilon \sim R_m^{-\frac{1}{2}}$ and $B^* \sim R_m^{\frac{1}{2}}$.

Busse (1975) estimated the velocity a by expanding about R_0, the critical Rayleigh number in the absence of a magnetic field, and computing the kinematically distorted field. For $\lambda = 1$ he obtained a modified form of the finite-amplitude expression in (3.11) and (3.12), with

$$R = R_0 + \tfrac{1}{2}\pi^4 a^2 + 34{\cdot}5Q(a/\zeta)^{-\frac{1}{2}} + O(a^3). \tag{3.16}$$

This result really represents the energy budget for the dynamical problem, normalized with respect to the viscous dissipation σa^2, for the rate of ohmic dissipation in a flux sheet of thickness ϵ, with a field B^*, is of order $R_m^{\frac{3}{2}} \sigma \zeta Q$. The estimate is valid for small a, for $\zeta \ll a$ and for Q sufficiently small that the field affects the magnitude but not the form of the velocity in (3.13).

From (3.16), Busse deduced that steady convection is possible with $R_{\min} \leqslant R < R^{(e)}$, for some $R_{\min} > R_0$, provided that the magnetic Reynolds number is sufficiently large. He observed that, for fixed Q, the function $R(a)$ defined by (3.16) reaches its minimum value $R_{\min}$ when

$$a = (17{\cdot}25\zeta^{\frac{1}{2}} Q/\pi^4)^{\frac{2}{5}}, \tag{3.17}$$

so that

$$R_{\min} = R_0 + \tfrac{5}{2}(17{\cdot}25\pi\zeta^{\frac{1}{2}} Q)^{\frac{4}{5}}. \tag{3.18}$$

Comparison of (3.18) with (3.3) shows that for ζ sufficiently small and Q sufficiently large $R_{\min} < R^{(e)}$, though it is likely that $R^{(o)} < R_{\min}$. In the regime where this result is valid steady convection is possible for all $R > R_{\min}$. Overstable modes should appear earlier and so there may be some hysteresis when R is slightly greater than $R_{\min}$. The behaviour of solutions in the R–a^2 plane is shown schematically in figure 1 (*b*). For a given value of $R > R_{\min}$, equation (3.16) yields two possible values of a^2 but the solutions on the lower branch should be unstable. It is tempting, as well as tidy, to link this unstable branch to the bifurcation at $R = R^{(e)}$, as sketched in the figure (cf. Proctor & Galloway 1978). This conjectured link is supported by the results of Knobloch *et al.* (1981). To confirm these predictions we turn to the numerical experiments.

4. Numerical experiments: flux expulsion and subcritical convection

The calculations described in this and the following section were designed to explore the transition from an almost linear to a thoroughly nonlinear regime and, in particular, to investigate the onset of steady finite-amplitude convection. All the results presented are for square cells ($\lambda = 1$) with $\sigma = 1$ and $\zeta \leqslant 1$. For each choice of Q and ζ a series of runs was made at different values of R. Initial conditions could be varied: runs were started either by perturbing the static solution or, preferably, by modifying a previously obtained solution. The calculations were pursued until solutions converged either to a steady state or (with one exception) to strictly periodic oscillations. Where necessary, the mesh interval was halved in order to ensure sufficient accuracy. On a mesh with $N_x = N_z = 24$ typical runs required from 2000 to 6000 timesteps, taking 4–12 minutes on an IBM 370/165. This paper presents results from over 100 runs, which are listed in the appendix.

The results can be presented either by plotting contours of the fields ψ (streamlines), ω, A (lines of force) and T (isotherms) or in terms of global measures of the flow. The global kinetic and magnetic energies are measured by the mean-square velocity

$$\langle u^2 \rangle = \lambda^{-1} \iint |\mathbf{u}|^2 \, dx \, dz = \lambda^{-1} \iint \psi \omega \, dx \, dz \tag{4.1}$$

and the mean-square magnetic field

$$\begin{aligned} \langle B^2 \rangle &= \lambda^{-1} \iint |\mathbf{B}|^2 \, dx \, dz \\ &= \lambda^{-1} \iint A j \, dx \, dz + \int_{x=1} A B_z \, dz. \end{aligned} \tag{4.2}$$

The efficiency of convection is measured by a normalized heat transport, the Nusselt number

$$N = \lambda^{-1} \int (wT - \partial T / \partial z) \, dx; \tag{4.3}$$

N is a function of z but should be constant in a steady state. The quantities $\langle u^2 \rangle$ and $\langle B^2 \rangle$, together with N evaluated at the top and bottom of the layer and the numerically largest values of each component of $\mathbf{u}$ and $\mathbf{B}$, could be monitored at every timestep of the calculation. All runs used in this paper, with corresponding values of N, are specified in the appendix.

Let us first consider the effect of a comparatively weak magnetic field. When $Q \lesssim 1$ the field has no dynamical effect. The velocity and temperature could be obtained from solutions of the ordinary Rayleigh–Bénard problem (e.g. Moore & Weiss 1973) and $\mathbf{B}$ could then be derived from the induction equation. For comparison with subsequent results N is plotted against R in figure 2(*a*) for the case when $Q \ll 1$. The only bifurcation is at $R_0 = 8\pi^4 \approx 779{\cdot}3$; thereafter, N increases monotonically with R. In a steady state, magnetic flux is expelled from most of the convecting region, when R_m is large, and concentrated at the lateral boundaries, as in earlier kinematic calculations.

Also shown in figure 2(*a*) are the very different results obtained with $Q = 100$, $\zeta = 0{\cdot}1$. Convection sets in as an oscillatory mode when $R = R^{(o)} \approx 1051$ and the peak values of the Nusselt number for oscillatory solutions are indicated in the figure.

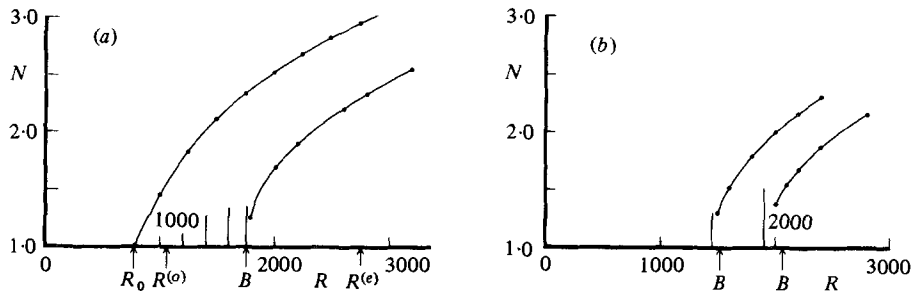

FIGURE 2. Subcritical convection with $\zeta^{\frac{1}{2}}Q < 50$. The Nusselt number N is plotted as a function of the Rayleigh number; the continuous lines connect stable steady solutions and the vertical bars indicate the maximum amplitudes of oscillatory solutions. (*a*) Convection in the absence of a magnetic field ($Q = 0$), with the steady branch bifurcating from R_0 and convection with $\zeta = 0{\cdot}1$, $Q = 100$. In the latter case the oscillatory branch bifurcates from $R^{(o)}$ and the steady branch, presumably, from $R^{(e)}$. The value of $R_{\min}$ calculated from (3.18) is indicated by the letter B. (*b*) As above but for $\zeta = 0{\cdot}05$, $Q = 100$ and 200.

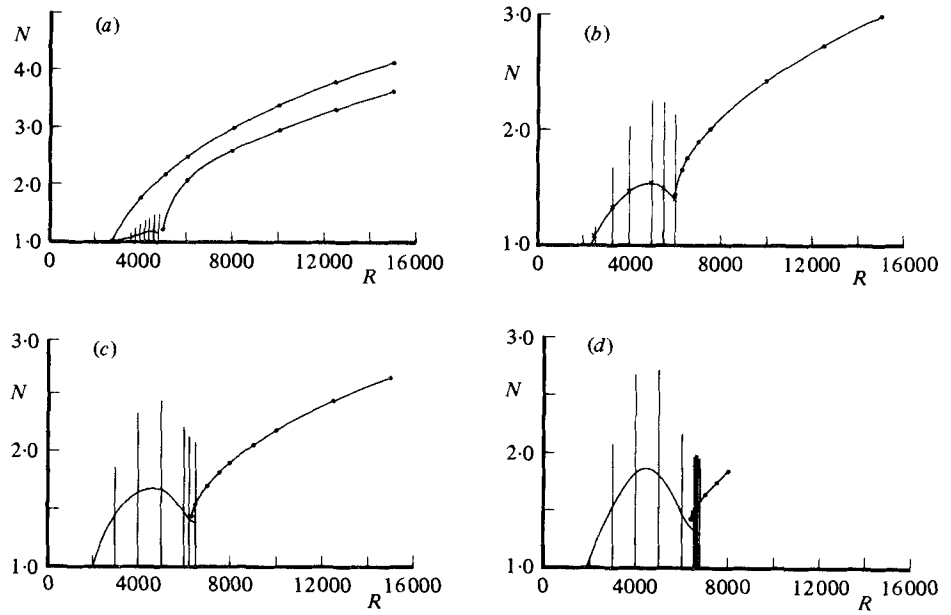

FIGURE 3. Convection with $\zeta Q = 100$; as for figure 2 except that the time-averaged value of the Nusselt number is also shown for the oscillatory solutions. (*a*) $\zeta = 1$ and 0·5, (*b*) $\zeta = 0{\cdot}2$, (*c*) $\zeta = 0{\cdot}1$, (*d*) $\zeta = 0{\cdot}05$.

Steady convection appears for $R > R_{\min} \approx 1780$, very close to the value of 1746 predicted by (3.18). From table 1 it can be seen that $R_{\min} < R^{(i)} < R^{(e)}$: steady convection is found in a parameter range where linear theory predicts oscillatory modes and well before the bifurcation at $R^{(e)}$. Figure 2(*b*) shows $N(R)$ for two further sets of runs, with $Q = 100, 200$ and $\zeta = 0{\cdot}05$. Once again, the agreement between the values of $R_{\min}$ predicted by Busse (1975) and those found by computation is extremely good, confirming the accuracy of each approach.

Inspection of the numerical results shows that, near $R = R_{\min}$, the stream function does not differ significantly from that in (3.13), that u varies linearly with x near

Q	ζ	$\zeta^{\frac{1}{2}}Q$	$R^{(o)}$	$R^{(i)}$	$R^{(e)}$	$R_{\min}$ Computed	$R_{\min}$ From (3·18)	$R_{\max}$
100	0·1	31·6	1051	1911	2753	1780	1746	1780
100	0·05	22·4	911	1591	2753	1480	1512	1500
200	0·05	44·7	963	2039	4727	1950	2054	2000
200	0·5	141	3233	4505	4727	4900	3982	4800
500	0·2	224	2306	5943	10649	5950	5400	6050
1000	0·1	316	2029	6446	20518	6300	6876	6550
2000	0·05	447	1895	6702	40258	6350	8824	6850
4000	0·025	632	1830	6834	79736	6400	11394	—

TABLE 1. The onset of steady convection.

$x = 0, 1$ and that $B_z(x, 0)$ and $B_z(x, 1)$ have approximately Gaussian profiles in the flux ropes, which are fairly broad. To this extent the solutions are qualitatively similar to those obtained when the magnetic field has no dynamical effect. Busse's treatment is, however, valid only for a restricted range of the parameters, such that $\zeta^{\frac{1}{2}}Q \lesssim 50$. When $\zeta^{\frac{1}{2}}Q \gg 100$ the values of $R_{\min}$ found from numerical experiments cease to agree with those obtained from (3.18), as can be seen from the results in table 1. In this new regime the solutions no longer have the same form; in particular, the Gaussian profile flattens until the field in the flux ropes becomes almost uniform.

5. Numerical experiments: exclusion of motion by the magnetic field

To investigate this fully nonlinear regime the development of steady convection was studied for different values of ζ while ζQ was held constant. (In dimensional terms this corresponds to varying η while B_0 is fixed.) For all these experiments $\zeta Q = 100$. Then, from (3.5), convection sets in as an oscillatory mode provided that $\zeta < 0{\cdot}6581$; when $\zeta = 0{\cdot}6581$, $R^{(o)} = R^{(i)} = R^{(e)} \approx 3779$. As $\zeta \to 0$, $R^{(o)} \to 1766$, from (3.6), while $R^{(i)} \to 6962$ and $R^{(e)}$ becomes infinite. Six series of runs were carried out, with $1 \geqslant \zeta \geqslant 0{\cdot}025$.

When $\zeta = 1$, steady convection occurs for all $R > R^{(e)} \approx 2753$. The bifurcation is supercritical and the Nusselt number increases monotonically with R, as shown in figure 3(*a*). As R increases, magnetic and thermal boundary layers are formed but the vorticity has no fine structure, as can be seen from figure 4(*a*). The streamlines are similar to those for the linear solution of (3.13) and the flow resembles that found in the absence of a magnetic field (Moore & Weiss 1973).

Table 1 lists values of $R^{(o)}$, $R^{(i)}$, $R^{(e)}$, $R_{\min}$ and $R_{\max}$ for the runs with $\zeta < 1$. Oscillatory solutions are found when $\zeta = 0{\cdot}5$ and their amplitude increases with R, as shown in figure 3(*a*). These finite-amplitude oscillations persist up to $R = 4800$, a value larger than $R^{(i)}$ and marginally greater than $R^{(e)}$. When $R = 5000$ steady convection appears with $N = 1{\cdot}21$ (for comparison, at the same value of R, $N = 2{\cdot}21$ when $\zeta = 1$). This steady solution was used to start another run at $R = 4800$, in order to investigate possible hysteresis, but oscillations developed once again. Similarly, when the oscillatory solution for $R = 4800$ was used to start a run with $R = 5000$ only steady convection was obtained. For this value of ζ, oscillatory convection occurs over a range $R^{(o)} < R \leqslant R_{\max}$ greater than that predicted by linear theory, and finite-amplitude

steady convection is possible only for $R \geqslant R_{\min} > R^{(e)}$. Apparently N still increases monotonically with R along the steady branch that bifurcates from the static solution at $R = R^{(e)}$. As we have already seen, the steady solution is unstable in the neighbourhood of $R^{(e)}$ and does not gain stability until $R \approx 5000$. This pattern of behaviour is consistent with that found by Knobloch *et al.* (1981) and by Knobloch & Proctor (1981).

For smaller values of ζ the pattern is quite different and steady convection appears while $R < R^{(e)}$. Figures 3(*b*) and 3(*c*) show N as a function of R for $\zeta = 0{\cdot}2$ and $\zeta = 0{\cdot}1$. When $\zeta = 0{\cdot}2$, small perturbations develop into finite-amplitude oscillations for $R \leqslant 6000$ but give rise to steady convection if $R \geqslant 6250$. A run with $R = 6000$, started from a steady solution at $R = 6500$, settled down to steady convection with $N = 1{\cdot}45$ but the steady solution gave way to oscillations at $R = 5900$. Conversely, a run with $R = 6100$, started from the oscillatory solution at $R = 6000$, settled down to steady convection. Thus a slight amount of hysteresis can occur. Similarly, when $\zeta = 0{\cdot}1$, oscillations persist until $R = 6500$ but steady solutions can be generated for $R \geqslant 6350$, with $N \geqslant 1{\cdot}44$.

As ζ is decreased, the oscillatory solutions grow in amplitude, though the average value of N at the end of the oscillatory branch is always less than that at the beginning of the steady branch. Both the peak value of N and its average value $\bar{N}$ have maxima before the oscillations disappear. Figure 3(*d*) shows results for $\zeta = 0{\cdot}05$. Steady convection is possible for $R \geqslant 6400$ while oscillations can be maintained up to $R = 6800$: the range of overlap, though modest, has increased and the transition from oscillatory to steady convection occurs when R is close to $R^{(i)}$, the value at which the eigenvalues of the linear problem cease to be complex. The runs at $R = 6400$ and $R = 6500$ with $N_x = 24$ were both repeated with $N_x = 48$ but there was no significant change in the Nusselt numbers (1·40 and 1·47 respectively). Finally, a single run with $R = 6500$, $\zeta = 0{\cdot}025$ again showed steady convection with $N = 1{\cdot}47$.

These results clearly demonstrate the existence of steady subcritical convection, with $R_{\min} \leqslant R < R^{(e)}$, provided $\zeta \leqslant 0{\cdot}2$. Moreover, both the value of $R_{\min}$ and the corresponding Nusselt number become independent of ζ as $\zeta \to 0$. For $\zeta Q = 100$, $R_{\min} \approx 6400$ and $N \approx 1{\cdot}40$ in this limit, so that $R^{(o)} < R_{\min} < R^{(i)} \ll R^{(e)}$. Table 1 also shows that $R_{\min}$ is much less than the value computed from (3.18), which increases as $\zeta^{-0{\cdot}4}$. In fact $R_{\min}$ apparently tends to a limit that is quite close to the limiting value of $R^{(i)}$, although the linear and nonlinear solutions are entirely different.

To obtain steady convection near $R_{\min}$ it is necessary to start from an adjacent steady-state solution. When $R < R_{\min}$ the motion slowly decays, without reversing, until an almost static state is reached. Only then do spasmodic oscillations start. (For R slightly greater than $R_{\max}$, on the other hand, there are irregular transient oscillations before the solution settles down towards a steady state.) Figure 4(*b*) shows the fields when R is slightly greater than $R_{\min}$ for $\zeta = 0{\cdot}025$, the smallest value that was used. (The sense of rotation in the eddy, which is arbitrary, is opposite to that in figure 4(*a*).) Note that the streamlines are concentrated near the centre of the cell and do not approach the lateral boundaries. The field is restricted to sheets which together fill more than a quarter of the cell, while the eddy is confined to the central region and motion is excluded from the flux sheets. Within these sheets thermal diffusion tends to make the vertical temperature gradient more uniform. The isotherms are therefore slightly inclined in the opposite sense to that in the central region. Hence there is a weak, thermally driven countercirculation in the flux sheets, whose effect on the lines

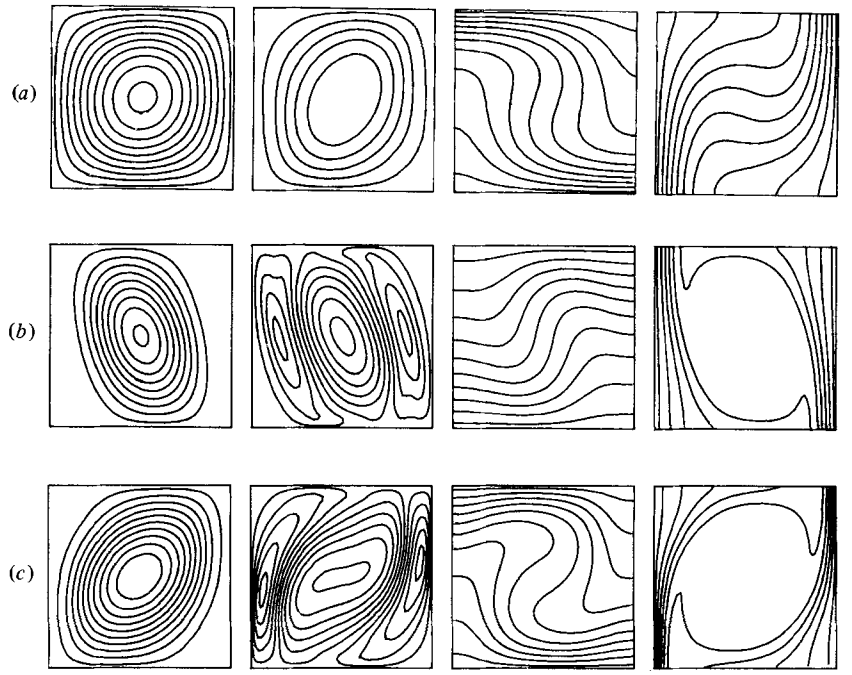

FIGURE 4. Steady convection with $\zeta Q = 100$. Contours of ψ (streamlines), ω, T (isotherms) and A (lines of force) for (*a*) $\zeta = 1$, $R = 6000$, (*b*) $\zeta = 0{\cdot}025$, $R = 6500$, (*c*) $\zeta = 0{\cdot}1$, $R = 15000$.

of force can just be detected. The fields for a more vigorously convecting case, with $N = 2{\cdot}64$, are shown in figure 4(*c*). The magnetic field is concentrated into narrower zones and the vorticity shows more structure than in figure 4(*b*).

In this regime, where $R_{\min}$ tends to a limit for $\zeta \ll 1$, the thickness of the flux sheet is also independent of ζ. Figures 5(*c*), (*d*), (*e*) and (*f*) show profiles of B_z in the flux sheet for $R \approx R_{\min}$ and $\zeta = 0{\cdot}2$, $0{\cdot}1$, $0{\cdot}05$ and $0{\cdot}025$, together with corresponding values of $u(x)$, compared with similar curves for $R = 6000$, $\zeta = 1$ in figure 5(*b*). When $\zeta = 1$, the horizontal component of the velocity still increases linearly across the flux sheet and the magnetic field has a Gaussian profile; as ζ decreases the field profile becomes flatter until, for $\zeta = 0{\cdot}025$, there is a local minimum at $x = 0$ caused by the slow counterflow within the flux sheet. At the same time u drops to zero where the field is strong and only rises in the narrow current sheet, where $|\partial B_z/\partial x|$ is large. Profiles of the vertical velocity show even more clearly how motion is excluded from the flux sheets. In figure 5(*a*) $w(x, \frac{1}{2})$ is plotted for $R = 6000$, $\zeta = 1$ and for $R = 6500$, $\zeta = 0{\cdot}025$, corresponding to the fields in figures 4(*a*) and (*b*) respectively. When $\zeta = 1$, w is a maximum at the edge of the cell and falls monotonically towards the centre but for $\zeta = 0{\cdot}025$ the vertical velocity is slightly negative at the edge, and increases at first slowly, then more rapidly, to reach a maximum near $x = 0{\cdot}3$. The run with $R = 15000$, $\zeta = 0{\cdot}1$ yields similar results. In the fully dynamic regime the flux sheets are almost stagnant and both components of the velocity approach zero at the sides of the cell. As x increases, w rises more rapidly than u but only reaches its maximum outside the flux sheet.

The half-width ϵ of the flux sheet can be defined as the value of x for which $|\partial B_z/\partial x|$ is a maximum. From figure 5 it can be seen that ϵ is approximately constant. For these runs $\epsilon \approx \frac{1}{8}$ and the field is amplified by a factor of around 4. (In dimensional terms,

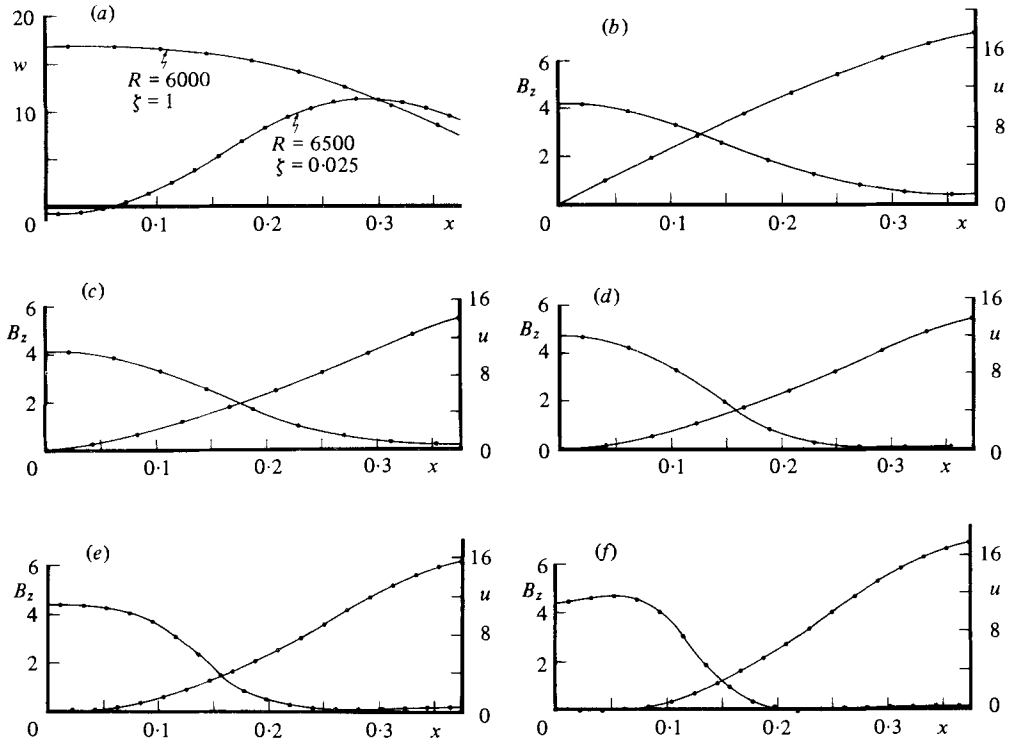

FIGURE 5. Stagnant flux sheets. Steady solutions with $\zeta Q = 100$: (*a*) $w(x, \frac{1}{2})$ for $\zeta = 1$, $R = 6000$ and $\zeta = 0{\cdot}025$, $R = 6500$; $B_z(x, 1)$ and $u(x, 1)$ for (*b*) $\zeta = 1$, $R = 6000$, (*c*) $\zeta = 0{\cdot}2$, $R = 6000$, (*d*) $\zeta = 0{\cdot}1$, $R = 6350$, (*e*) $\zeta = 0{\cdot}05$, $R = 6400$, (*f*) $\zeta = 0{\cdot}025$, $R = 6500$.

since B_0 is fixed, it follows that both ϵ and the peak field B^* are independent of η when $R = R_{\min}$.) Only the thickness of the current sheet depends on the magnetic diffusivity. Since both $R_{\min}$ and N are independent of η when $\zeta \ll 1$, the velocity too must approach a limiting form. In these results the ratio of the Alfvén speed $(\sigma\zeta Q)^{\frac{1}{2}} B^*$ to the maximum vertical velocity is about 4. For $R > R_{\min}$, B^* remains approximately independent of ζ, though N drops slightly as ζ is decreased. The results are insufficient to demonstrate the presence of any asymptotic regime but for a given ζ they can be fitted by assuming that $N \propto R^{\frac{1}{2}}$.

6. Nonlinear oscillations

The periodic solutions display a considerable variety of behaviour and the transition from oscillatory to steady convection can be very complicated. Much of this rich structure can be clarified by close study of the time-dependent results. Details of the transition to steady convection and of bifurcations from the oscillatory solutions can be confirmed by studying a simpler system of five coupled ordinary differential equations, derived from (2.12), (2.13) and (2.14), whose solutions mimic the behaviour of solutions to the full two-dimensional problem (Knobloch *et al.* 1981).

Near the onset of overstability the nonlinear oscillations differ only slightly from the eigenfunctions of the linear problem. Figure 6 shows the time-dependent fields at six successive stages during half of a full cycle, for $Q = 1000$, $\zeta = 0{\cdot}1$ and $R = 3000$.

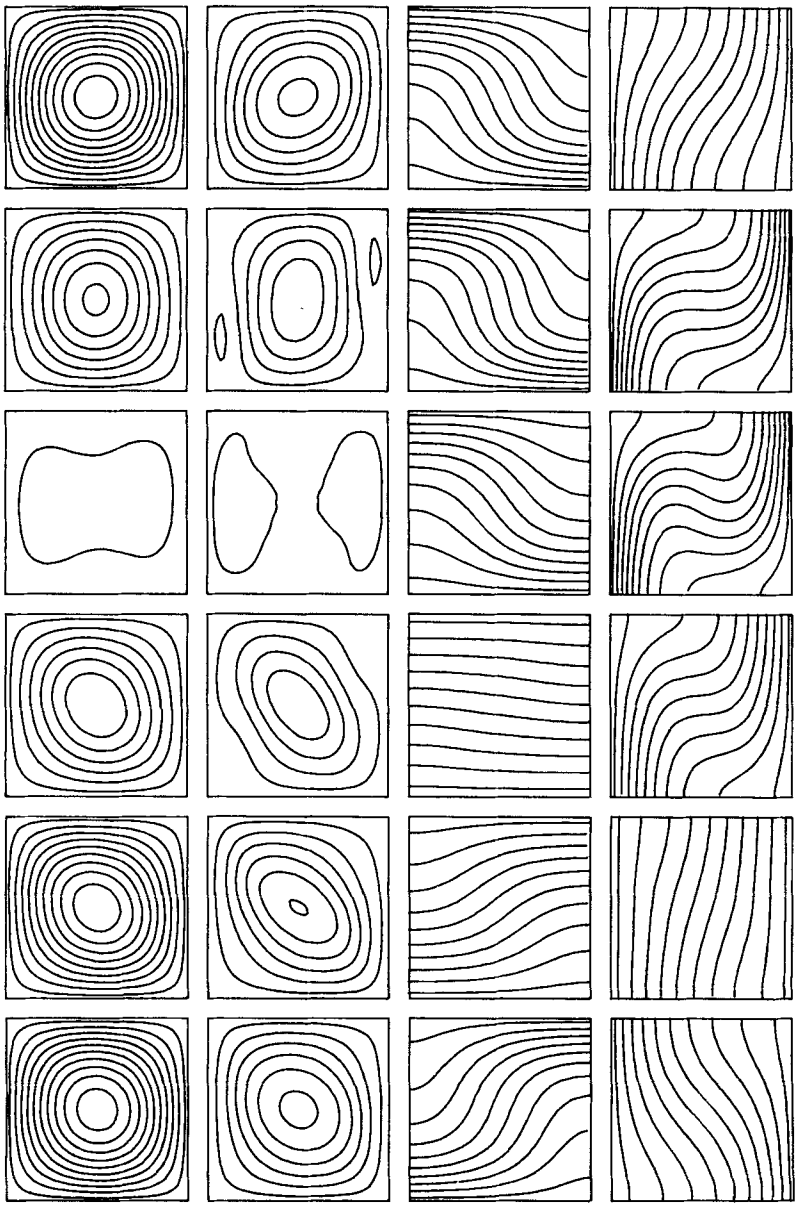

FIGURE 6. Oscillatory solutions for $\zeta Q = 100$, $\zeta = 0{\cdot}1$. Contours of ψ, ω, T and A at six equally spaced intervals in time during a half-cycle, starting when the velocity is a maximum, for $R = 3000$. The contour levels remain fixed throughout the sequence.

Initially the motion is clockwise and the velocity is at a maximum. The streamlines scarcely differ from those given by (3.13), while the vorticity rises to a flat extremum at the centre of the cell and shows no fine structure near the sides. As the oscillation proceeds the field is distorted but no isolated sheets of flux appear. Some structure appears in the vorticity as the flow reverses and the sense of motion becomes anti-clockwise; the maximum distortion of the field coincides approximately with the

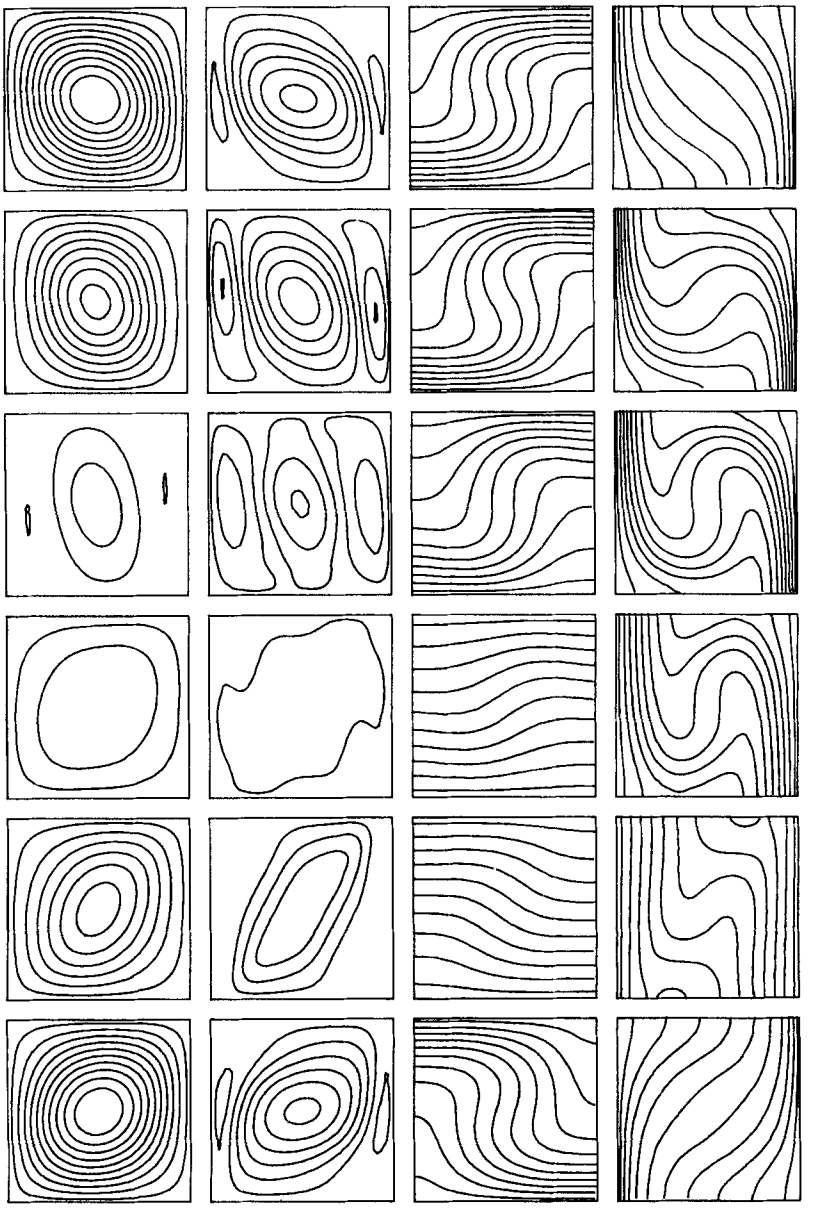

FIGURE 7. As for figure 6 but with $R = 5000$.

moment when the flow is halted and the field is almost uniform as the velocity approaches its maximum. This pattern of behaviour is shown more clearly in figure 9(*a*), where the Nusselt number N, the mean-square velocity $\langle u^2 \rangle$ and the excess magnetic energy, measured in the same units as $\langle u^2 \rangle$,

$$\langle \Delta B^2 \rangle = (\sigma\zeta Q)\,[\langle B^2 \rangle - 1] = (\sigma\zeta Q)\,\langle |\mathbf{B} - \mathbf{e}_z|^2 \rangle, \tag{6.1}$$

are plotted as functions of time for one complete oscillation, starting at the instant when $\langle u^2 \rangle$ is a minimum. The variation is almost sinusoidal: kinetic energy is transformed into magnetic energy and the velocity drops to zero as the field is compressed.

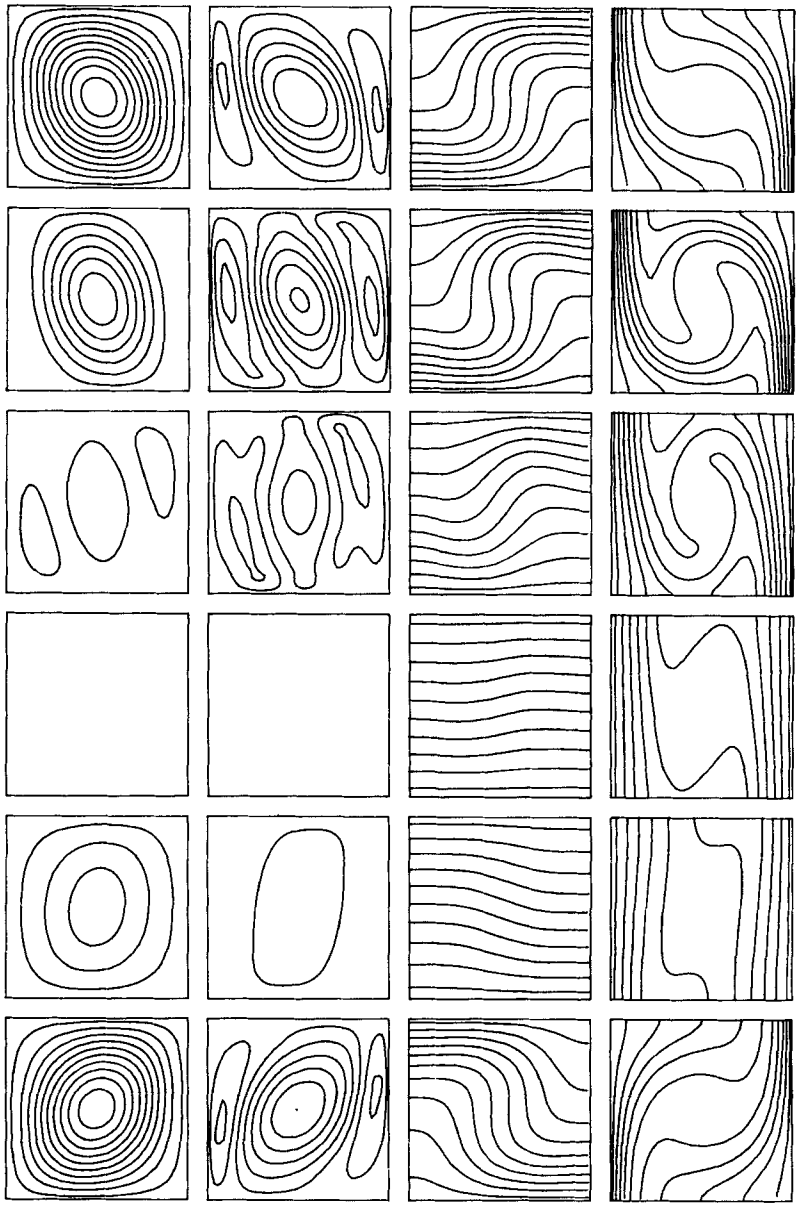

FIGURE 8. As for figure 6 but with $R = 6500$.

The change in magnetic energy is, however, about twice the change in the kinetic energy.

As R is increased, the oscillations develop more structure. Two further cases, with the same values of Q and ζ but with $R = 5000$ and $R = 6500$, are shown in figures 7 and 8, with the corresponding behaviour of global quantities displayed in figures 9(*b*) and (*c*). The contours in figure 7 show that the field is more thoroughly distorted and, correspondingly, more dynamically active. As the field lines are compressed, two zones of countervorticity, generated by the Lorentz torque, appear and gradually expand

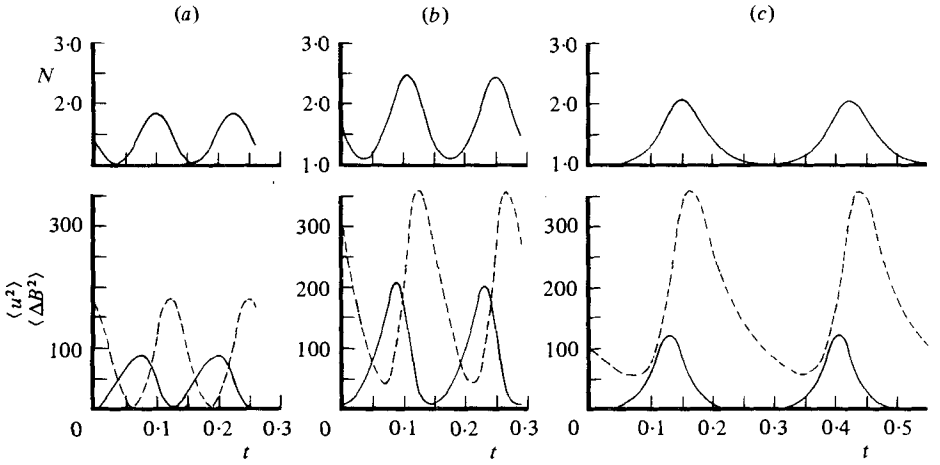

FIGURE 9. Variation of global quantities in the oscillatory solutions illustrated above. N, $\langle u^2\rangle$ (solid line) and $\langle \Delta B^2\rangle$ (broken line) as functions of time for $\zeta Q = 100$, $\zeta = 0{\cdot}1$ and (*a*) $R = 3000$, (*b*) $R = 5000$, (*c*) $R = 6500$.

towards the centre until the flow there is reversed. This nonlinear behaviour differs from that in figure 6 as well as from that of the linear solutions. Figure 9 (*b*) shows that the oscillations have increased in period as well as amplitude. The kinetic energy falls more rapidly than it rises and the peaks are sharper than the troughs.

These changes are much more marked when $R = 6500$, just before the transition to steady convection at $R = R_{\max}$. The period is more than double that for $R = 3000$ and the oscillations are spasmodic: bursts of activity are separated by long static intervals, when the kinetic energy is extremely small, as can be seen from figure 9 (*c*). The peak value of $\langle \Delta B^2\rangle$ remains as high as in figure 9 (*b*) but the maxima of N and $\langle u^2\rangle$ are reduced. The sequence of contours in figure 8 show that the field is dynamically more important. Flux is rapidly concentrated at the edges of the cell until the Lorentz force halts the motion. The lines of force straighten out rapidly, on the Alfvénic timescale, so that $(\mathbf{B}.\nabla)\mathbf{B}$ is everywhere small and the Lorentz force can be balanced by a pressure gradient. The field gradually grows more uniform, on a diffusive timescale, until the next burst of activity ensues. Despite the period of stasis, the motion flips from one direction to the other and the numerical solutions are almost exactly periodic. The transient effects of the initial conditions do, however, take a long time to decay and this run had to be continued for ten full cycles to confirm the regularity of the oscillations.

The period P of the oscillations in figure 9 is the interval between alternate maxima (or minima) of N, $\langle u^2\rangle$ or $\langle \Delta B^2\rangle$, since the flow reverses in between. It is clear from this figure that P increases with increasing R: figure 10 shows the ratio of P to P_0, the period at $R = R^{(o)}$, as a function of R for two other series of runs with $\zeta Q = 100$. When $\zeta = 0{\cdot}5$, P/P_0 increases monotonically from unity at $R^{(o)}$ to a value of 3·1 just before the oscillations disappear. When $\zeta = 0{\cdot}05$, the ratio first decreases to a minimum value around 0·8 and then rises until oscillations give way to steady motion. The results for $\zeta = 0{\cdot}5$ suggest that P/P_0 may become infinite for a finite value of R and the model calculations of Knobloch *et al.* (1981) have shown that the oscillatory branch can terminate on the unstable portion of the steady branch at $R = R_{\max}$, when the period

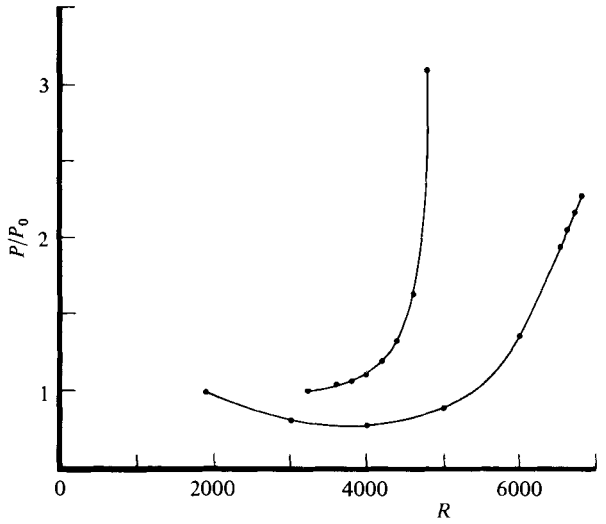

FIGURE 10. Variation of the period of oscillatory solutions. P/P_0 is plotted against R for $\zeta Q = 100$ and $\zeta = 0{\cdot}5$ (narrow range), $\zeta = 0{\cdot}05$ (broader curve).

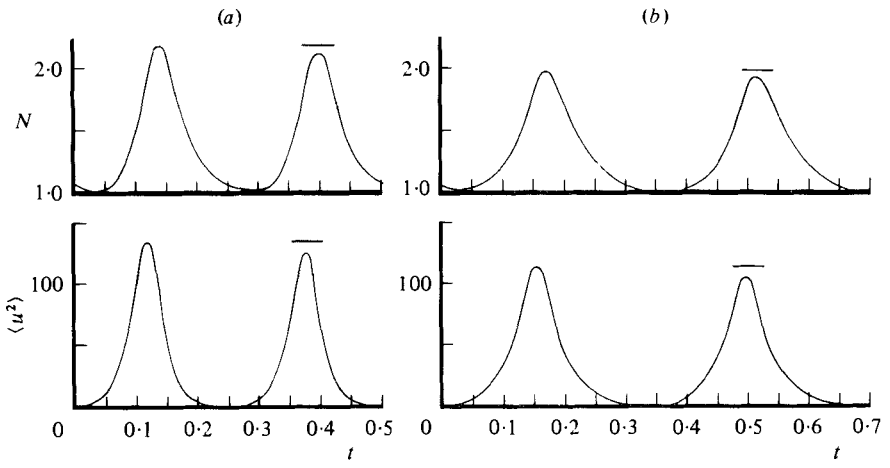

FIGURE 11. Asymmetrical oscillations. N and $\langle u^2 \rangle$ plotted as functions of time for a complete cycle with $\zeta Q = 100$ and (*a*) $\zeta = 0{\cdot}2$, $R = 6000$, (*b*) $\zeta = 0{\cdot}05$, $R = 6800$. The distance between the lower peaks and the horizontal bar shows the extent of the asymmetry.

is infinite. Whether P becomes infinite or not in this particular case depends on whether the unstable steady branch doubles back or retains a positive slope for all $R > R^{(e)}$, and this cannot be determined from figure 3(*a*).

When $\zeta = 0{\cdot}05$ the steady branch has to double back and $R_{\min} \ll R^{(e)}$. Yet figure 10 suggests that the period remains finite as R approaches $R_{\max}$. Close inspection shows that the oscillations have changed. The original equations have no preference for clockwise or anticlockwise motion and this symmetry is preserved when oscillations first appear. For the solutions shown in figures 6, 7 and 8 each half-cycle is the mirror image of its predecessor. Just before $R_{\max}$, however, there is a bifurcation at which these symmetrical oscillations lose stability to asymmetrical oscillations, with a slight

preference for one or the other sense of motion. The period P does not change at this bifurcation but the loss of symmetry means that successive peaks in N, $\langle u^2 \rangle$ or $\langle \Delta B^2 \rangle$ are no longer identical and the period of these quadratic quantities jumps from $\frac{1}{2}P$ to P. The differences are small but they can be clearly seen in figures 11 (*a*) and (*b*), where N and $\langle u^2 \rangle$ are plotted for a full cycle for the last oscillatory solutions with $\zeta = 0{\cdot}2$ and $\zeta = 0{\cdot}05$ respectively. In figure 11 (*b*) the maxima of N are 1·98 and 1·93, and the maxima of $\langle u^2 \rangle$ are 114 and 106; the corresponding variation in $\langle \Delta B^2 \rangle$ is less than 1 %. This pattern of asymmetric oscillations was maintained for five full cycles.

These results imply that for $\zeta Q = 100$, $\zeta \leqslant 0{\cdot}2$ the transition from periodic to steady solutions at $R = R_{\max}$ is preceded by a bifurcation from symmetrical to asymmetrical oscillations. An analogous bifurcation appears in the truncated system investigated by Knobloch *et al.* (1981) and similar bifurcations occur in other nonlinear systems. In some cases, including the model studied by Da Costa *et al.* (1981), this bifurcation to asymmetry may be followed by a sequence of bifurcations, at each of which the period doubles, until the solution becomes aperiodic after the accumulation point. The numerical experiments described here showed no signs of period doubling. In one case ($Q = 100$, $\zeta = 0{\cdot}1$, $R = 1750$) the oscillations had not settled down to being periodic when the run was terminated; in all other cases periodic solutions were eventually obtained. Irregular time-dependent behaviour is, however, more common at higher values of R and Q, as shown by the runs described in part 2.

7. Subcritical steady convection

For astrophysical applications it is important to establish the lowest value of the Rayleigh number for which steady convection is allowed. As can be seen from figure 4 (*b*), the form of the nonlinear solutions depends on the competition between the thermally driven circulation and the counterflow driven by magnetic fields in the flux sheets. The vorticity contours show a central zone with negative vorticity flanked by two regions with (positive) countervorticity, centred on the current sheets where the field strength increases. In this case the flow is excluded from the flux sheets. On the other hand, if Q is sufficiently small the field has a Gaussian profile and its peak value B^* is limited by diffusion. The extent of this kinematic regime can be estimated by the following simple argument (Galloway *et al.* 1978). We suppose that the Reynolds number U/σ is small; although this is not consistent with setting $\sigma = 1$ other two-dimensional calculations (Peckover & Weiss 1978) have shown that advection of vorticity has little qualitative effect on the solutions. For steady motion the velocity can then be separated into a part $\mathbf{u}_0$ (with vorticity ω_0) that is generated by the buoyancy force and a part $\mathbf{u}_1$ (with vorticity ω_1) that is generated by the Lorentz force. From (2.14),

$$\nabla^2 \omega_0 = R\,\partial T/\partial x, \quad \nabla^2 \omega_1 = -\zeta Q \mathbf{B} \cdot \nabla j. \tag{7.1}$$

Let U_0, U_1 be the maximum numerical values of the vertical components of $\mathbf{u}_0$, $\mathbf{u}_1$ and let ϵ be the half-width of the flux sheet. Then an order-of-magnitude calculation shows that

$$U_1 \sim \epsilon B^{*2} \zeta Q \sim \zeta Q/\epsilon. \tag{7.2}$$

The eddy is excluded from the flux rope when U_1 is comparable with U_0. In the fully dynamical regime, therefore,

$$\epsilon \sim \zeta Q/U_0, \tag{7.3}$$

which is independent of η. Now $\epsilon \sim (U/\zeta)^{-\frac{1}{2}}$ in the kinematic regime, from (3.14), and so the transition from the kinematic to the dynamic regime occurs when

$$U \sim (\zeta^{\frac{1}{2}}Q)^2. \tag{7.4}$$

Between the kinematic regime, where the Lorentz force is negligible, and the fully dynamic regime, where motion is excluded from the flux ropes, there is a transitional, weakly dynamic regime in which the concentrated field retains an approximately Gaussian profile in the flux ropes. From (7.4), the fully dynamic regime, with stagnant flux sheets in which the field has a top-hat profile, occurs only if $Q \gg R_m^{\frac{1}{2}} \gg 1$. For square cells, when $Q \gg 1$ and $\zeta \ll 1$, steady convection first appears at $R = R_{\min} < R^{(e)}$ with the field already concentrated into isolated sheets and with a finite velocity $U_{\min}$ (as in the cases described in § 4 and § 5 above). Then the field has an approximately Gaussian profile for $R > R_{\min}$ provided that $U_{\min} \gtrsim \zeta Q^2$. In the numerical experiments steady convection appeared with $1 < N \lesssim 3$ and $U_{\min} \sim 10$. Hence the field retains a Gaussian profile if $Q \lesssim \zeta^{-\frac{1}{2}}$. In particular, for the weakly dynamic regime discussed by Busse (1975) the velocity $U_{\min} \sim (\zeta^{\frac{1}{2}}Q)^{\frac{2}{3}}$, from (3.17), and so the treatment holds only if $\zeta^{\frac{1}{2}}Q$ is sufficiently small. The results in table 1 indicate that the transition from a weakly dynamic to a fully dynamic regime at $R = R_{\min}$, which corresponds to a transition from Gaussian to top-hat profiles in the flux ropes, occurs when $\zeta^{\frac{1}{2}}Q \approx 50$.

For $\zeta \ll 1$ and $\zeta^{\frac{1}{2}}Q \gtrsim 100$ steady convection sets in with the field confined to stagnant flux sheets, which occupy about a quarter of the cell. A comparison of figures 4(*b*) and (*c*) show that these sheets become more slender as the Rayleigh number is increased. In this fully dynamical regime the convecting region is separated from regions with strong fields by narrow current sheets across which the velocity drops to zero. In effect, the magnetic field changes the lateral boundary conditions for the convecting region. The current sheets exert a net tangential stress such that both components of $\mathbf{u}$ vanish at the sides of the eddy, and motion in the field-free region could be modelled by adopting fixed lateral boundaries while the horizontal boundaries remain free. For a given value of ϵ the velocity and hence the temperature distribution depend only on R. Since $\mathbf{u}_0$ is determined by the temperature, it follows from (7.3) that ζQ is constant. Conversely, if R is given and ζQ held constant then ϵ and B^* are independent of ζ. (In dimensional terms, ϵ depends on B_0 but not on η.) The thickness of the current sheet does depend on ζ and adjusts itself until ohmic losses are equal to the difference between the rate of working of the buoyancy force and the rate of viscous dissipation: thus this thickness is proportional to ζ.

It is difficult to provide even a crude model of the dynamic regime, for the flux sheets need not be narrow compared with thermal plumes even if $\zeta \ll 1$. It is, however, possible to estimate $R_{\min}$. Expulsion of magnetic flux allows convection at the centre of the cell but the flux ropes become dynamically more active as they are compressed. Suppose that the thermal plumes have half-widths δ, where $\epsilon < \delta < 1$. Then, from (7.1),

$$U_0 \sim \delta R \tag{7.5}$$

and, from (7.2), $U_0 \sim U_1$ when

$$R = \zeta Q/(\delta\epsilon) > \zeta Q. \tag{7.6}$$

Hence steady convection should appear with moderately wide flux ropes so that

$$R_{\min} \sim \zeta Q. \tag{7.7}$$

As ζQ increases $R_{\min}$ also rises and the thermal plumes grow narrower, so that $\delta \to \epsilon$. The numerical results in this paper and in Part 2 provide some support for (7.7), though they are not yet in the asymptotic regime. At $R = R_{\min}$, $\epsilon \sim \frac{1}{4}$ but thermal plumes are not yet fully formed even when $R_{\min} = 10^5$, although the value of N does rise slowly as ζQ is increased.

Previous attempts to estimate the effective Rayleigh number for the onset of vigorous convection have also yielded criteria similar to (7.7). For a perfect fluid there is the stability criterion of (3.2), which can be derived by balancing the buoyancy torque against the couple exerted by the field (Cowling 1953, 1957). Danielson (1961) supposed that vigorous steady convection appeared when $R = R^{(i)}$, at the transition from oscillatory to direct modes; from (3.10), this yields the same result when $\zeta Q \gg 1$. Criteria derived from linear theory may be misleading. Nonlinear results are harder to establish: Biermann (1941) suggested that the magnetic field in a sunspot is able to suppress convection because the magnetic energy density exceeds the kinetic energy density of ambient convection (an idea which he ascribed to Cowling). More precisely, the field becomes dynamically important when the Maxwell stresses are comparable with the Reynolds stresses (Cowling 1953). Balancing the kinetic energy, estimated from the reduced free-fall speed, against the energy in the magnetic field gives equation (7.7) again (Weiss 1964). None of these arguments allows for the formation of isolated flux tubes, which are the most obvious feature of actual nonlinear solutions. Still, it is obvious on dimensional grounds that any simple argument must end up with the same result. In fact, $R_{\min}$ is close to $R^{(i)}$, at least for $\zeta Q \lesssim 500$.

The behaviour described above is 'subcritical', in the sense that steady convection occurs for $R < R^{(e)}$, but $R_{\min} > R^{(o)}$ in all the numerical results. It is of interest to discover whether nonlinear steady convection can occur at Rayleigh numbers less than that for the onset of overstability when $\zeta < 1$. If so, linear theory may be totally misleading. Busse (1975) conjectured that $R_{\min}$ might be less than $R^{(o)}$ for large Q and analogous behaviour has been demonstrated for double-diffusive convection (Huppert & Moore 1976). It seems unlikely that this can happen when $\lambda = \sigma = 1$, for $R^{(o)} \to \frac{1}{2}R^{(i)}$ as $\zeta Q \to \infty$, from (3.7) and (3.10). Indeed, $R_{\min}$ is never significantly less than $R^{(i)}$ in the regimes investigated here. On the other hand, the effect of increasing σ is to raise $R^{(o)}$ and, in the limit when $\sigma \gg 1$, $R^{(o)} \to R^{(i)}$. In that case, there may be a range of Q for which $R_{\min}$ is somewhat less than $R^{(o)}$; if so, the difference will still be fairly small.

8. Conclusion

The numerical experiments described in this paper provide an answer to the question: what field strength is needed to inhibit heat transport by convection? In a fluid with $\kappa \gg \eta$ magnetic flux is concentrated into isolated sheets or tubes which are embedded in the thermal plumes, and the dynamical effect of the field depends on the magnitude of Q. Provided that $\zeta^{\frac{1}{2}}Q \lesssim 1$, steady convection occurs with R not much greater than R_0, the critical Rayleigh number in the absence of a magnetic field. For $1 \lesssim \zeta^{\frac{1}{2}}Q \lesssim 50$, steady convection is possible if R exceeds the critical value $R_{\min}$ in (3.18), given by Busse (1975), and the field profile is approximately Gaussian. Once $\zeta^{\frac{1}{2}}Q \gtrsim 100$ the flux tubes become dynamically active. For $Q > Q_0$, convection first appears as periodic oscillations but the Nusselt number remains low until steady con-

vection takes over at $R = R_{\min} \sim \zeta Q$. In dimensional terms, steady convection is suppressed if

$$B_0^2/\mu\rho_0 \gtrsim g\alpha\,\Delta T d, \tag{8.1}$$

i.e. if the Alfvén speed is significantly greater than the reduced free-fall speed.

In this dynamical regime, magnetic flux is expelled from the convective eddies and concentrated into isolated sheets, from which the motion is excluded. The full extent of this regime, including the transition to a kinematic regime for large R, will be explored in Part 2. That paper also describes the effect of varying the cell width λ and the development of solutions that are spatially asymmetric. Many features of these two-dimensional results occur also in a cylindrical configuration (Galloway 1977, 1978; Galloway & Moore 1979). Proctor & Galloway (1978) have also explored the curious behaviour of $R_{\min}$ when Q is relatively small. The principal difference between the two-dimensional and axisymmetric configurations is that in the latter motion can be excluded from a central flux tube without appreciably reducing the external flow. In three dimensions, therefore, heat transport may scarcely be affected by the formation of flux ropes at the centres and corners of convection cells.

The oscillatory solutions display a rich variety of behaviour, some of which is reproduced in the model calculations of Knobloch *et al.* (1981) and Knobloch & Proctor (1981). In magnetoconvection buoyancy competes with the stabilizing effect of a magnetic field, which is relatively weaker when the field is confined to isolated tubes. Similarly, the stabilizing effect of rotation is reduced by concentrating gradients of angular momentum and that of a solute is diminished by restricting gradients in concentration to horizontal boundary layers. Of the various double-diffusive configurations that have been studied (Spiegel 1972), thermosolutal convection has attracted most attention. Huppert & Moore (1976) found many features of the problem discussed here, including a similar 'subcritical' transition from oscillatory to steady motion, accompanied by a more dramatic jump in heat transport; they also observed a bifurcation from symmetrical to asymmetrical oscillations, which was followed by a transition to aperiodic oscillations. There are important differences too: the solutal concentration is a scalar and makes a linear contribution to the equations of motion, whereas the Lorentz force is quadratic in $\mathbf{B}$, which is itself a solenoidal vector field. Solute plumes, unlike magnetic flux tubes, grow less dynamically active as they are compressed. The Lorentz force makes magnetoconvection a fascinating paradigm for the study of double-diffusive systems. This paper shows that, with the aid of numerical experiments, its rich nonlinear behaviour can be analysed and understood.

I am most grateful to Dr D. R. Moore for advice and help in writing the program and to Dr J. M. Wheeler for assistance in running the jobs. I am also grateful for comments and suggestions from F. H. Busse, D. J. Galloway, L. N. Howard, E. Knobloch, W. V. R. Malkus, R. S. Peckover, H. U. Schmidt, A. M. Soward and E. A. Spiegel. This research was supported by a grant from the Science Research Council and the paper was largely written during the GFD Summer Program at Woods Hole Oceanographic Institution and at the Harvard–Smithsonian Center for Astrophysics.

Appendix

The list below specifies the values of R, Q and ζ for nearly all of the numerical experiments. In each case $\lambda = 1$, $\sigma = 1$; $N_x = 24$ unless stated otherwise. Values of R are followed by corresponding values of the Nusselt number in brackets; light-face figures indicate the maximum and, where appropriate, the average values of N for oscillatory convection, bold-face values are for steady convection. The symbol a denotes asymmetric oscillations, while s indicates that a run, started either from a small perturbation or from the last oscillatory solution, settled down to steady convection, and **o** indicates that a run started from the first steady solution developed into oscillations.

$Q = 0$: 1000 (**1·46**), 1250 (**1·83**), 1500 (**2·11**), 1750 (**2·33**), 2000 (**2·52**), 2250 (**2·68**), 2500 (**2·82**), 2750 (**2·94**), 3000 (**3·06**), 3500 (**3·27**).

$Q = 100$, $\zeta = 0{\cdot}1$: 1200 (1·11), 1400 (1·27), 1600 (1·33), 1750 (a 1·30/1·37; **o**), 1800 (s; **1·25**), 2000 (**1·70**), 2200 (**1·90**), 2600 (**2·20**), 2800 (**2·32**), 3200 (**2·54**).

$Q = 100$, $\zeta = 0{\cdot}05$: 1450 (1·3; **o**), 1500 (**1·30**), 1600 (**1·53**), 1800 (**1·80**), 2000 (**2·00**), 2200 (**2·17**), 2400 (**2·32**).

$Q = 200$, $\zeta = 0{\cdot}05$: 1900 (1·52; **o**), 2000 (**1·37**), 2100 (**1·55**), 2200 (**1·68**), 2400 (**1·87**), 2800 (**2·16**).

$Q = 100$, $\zeta = 1$: 4000 (**1·77**), 5000 (**2·21**), 6000 (**2·54**), 8000 (**3·01**), 10000 (**3·37**), 12500 (**3·76**), 15000 (**4·11**).

$Q = 200$, $\zeta = 0{\cdot}5$: 3600 (1·16, 1·08), 3800 (1·24, 1·11), 4000 (1·31, 1·13), 4200 (1·37, 1·16), 4400 (1·42, 1·17), 4600 (1·46, 1·17), 4800 (1·49, 1·14; **o**), 5000 (s; **1·21**), 6000 (**2·09**), 8000 (**2·59**), 10000 (**2·93**), 12500 (**3·29**), 15000 (**3·62**).

$Q = 500$, $\zeta = 0{\cdot}2$: 2500 (1·16, 1·08), 3250 (1·67, 1·32), 4000 (2·04, 1·49), 5000 (2·26, 1·55), 5500 (2·24, 1·49), 5900 (**o**), 6000 (a 2·14/2·19, 1·40; **1·45**), 6100 (s; **1·58**), 6250 (**1·66**), 6500 (**1·76**), 7000 (**1·90**), 7500 (**2·02**), 10000 (**2·42**), 12500 (**2·72**), 15000 (**2·99**).

$Q = 1000$, $\zeta = 0{\cdot}1$: 3000 (1·86, 1·42), 4000 (2·33, 1·65), 5000 (2·45, 1·68), 6000 (2·21, 1·48), 6250 (2·13, 1·41; **o**), 6350 (**1·44**), 6500 (2·08, 1·38; **1·54**), 6600 (s), 7000 (**1·70**), 7500 (**1·83**), 8000 (**1·91**), 9000 (**2·07**), 10000 (**2·20**); $N_x = 48$: 12500 (**2·45**), 15000 (**2·64**).

$Q = 2000$, $\zeta = 0{\cdot}05$: 3000 (2·07, 1·52), 4000 (2·66, 1·83), 5000 (2·70, 1·81), 6000 (2·16, 1·50), 6300 (o), 6400 (**1·43**), 6500 (1·97, 1·34; **1·49**), 6600 (1·97, 1·33), 6700 (1·97, 1·31), 6800 (*a* 1·93/1·98, 1·29), 6900 (*s*; **1·62**), 7000 (**1·64**), 7500 (**1·75**), 8000 (**1·84**); $N_x = 48$: 6400 (**1·40**), 6500 (**1·47**).

$Q = 4000$, $\zeta = 0{\cdot}025$: $N_x = 48$: 6500 (**1·47**).

REFERENCES

BIERMANN, L. 1941 Der gegenwärtige Stand der Theorie konvektiver Sonnenmodelle. *Vierteljahrschr. Astr. Ges.* **76**, 194–200.

BUSSE, F. H. 1975 Nonlinear interaction of magnetic field and convection. *J. Fluid Mech.* **71**, 193–206.

CHANDRASEKHAR, S. 1952 On the inhibition of convection by a magnetic field. *Phil. Mag.* **43** (7), 501–532.

CHANDRASEKHAR, S. 1961 *Hydrodynamic and Hydromagnetic Stability*. Clarendon.

CLARK, A. 1965 Some exact solutions in magnetohydrodynamics with astrophysical applications. *Phys. Fluids* **8**, 644–649.

CLARK, A. 1966 Some kinematical models for small-scale solar magnetic fields. *Phys. Fluids* **9**, 485–492.

CLARK, A. & JOHNSON, A. C. 1967 Magnetic field accumulation in supergranules. *Solar Phys.* **2**, 433–440.

COWLING, T. G. 1953 Solar electrodynamics. In *The Sun* (ed. G. P. Kuiper), pp. 532–591. University of Chicago Press.

COWLING, T. G. 1957 *Magnetohydrodynamics*. Interscience.

DA COSTA, L. N., KNOBLOCH, E. & WEISS, N. O. 1981 Oscillations in double-diffusive convection. *J. Fluid Mech.* (to appear).

DANIELSON, R. E. 1961 The structure of sunspot penumbras. II. Theoretical. *Astrophys. J.* **134**, 289–311.

GALLOWAY, D. J. 1977 Axisymmetric convection with a magnetic field. In *Problems of Stellar Convection* (ed. E. A. Spiegel & J.-P. Zahn), pp. 188–194. Springer.

GALLOWAY, D. J. 1978 The origin of running penumbral waves. *Mon. Not. Roy. Astron. Soc.* **184**, 49P–52P.

GALLOWAY, D. J. & MOORE, D. R. 1979 Axisymmetric convection in the presence of a magnetic field. *Geophys. Astrophys. Fluid Dyn.* **12**, 73–106.

GALLOWAY, D. J., PROCTOR, M. R. E. & WEISS, N. O. 1978 Magnetic flux ropes and convection. *J. Fluid Mech.* **87**, 243–261.

GALLOWAY, D. J. & WEISS, N. O. 1981 Convection and magnetic fields in stars. *Astrophys. J.* **243**, 945–953.

GIBSON, R. D. 1966 Overstability in the magnetohydrodynamic Bénard problem at large Hartmann numbers. *Proc. Camb. Phil. Soc.* **62**, 287–299.

HUPPERT, H. & MOORE, D. R. 1976 Nonlinear double-diffusive convection. *J. Fluid Mech.* **78**, 821–854.

KNOBLOCH, E. & PROCTOR, M. R. E. 1981 Nonlinear periodic convection in double-diffusive systems. *J. Fluid Mech.* **108**, 291–316.

KNOBLOCH, E., WEISS, N. O. & DA COSTA, L. N. 1981 Oscillatory and steady convection in a magnetic field. *J. Fluid Mech.* (to appear).

MALKUS, W. V. R. & VERONIS, G. 1958 Finite amplitude cellular convection. *J. Fluid Mech.* **4**, 225–260.

MOORE, D. R., PECKOVER, R. S. & WEISS, N. O. 1973 Difference methods for time-dependent two-dimensional convection. *Comp. Phys. Comm.* **6**, 198–220.

MOORE, D. R. & WEISS, N. O. 1973 Two-dimensional Rayleigh–Bénard convection. *J. Fluid Mech.* **58**, 289–312.

PARKER, E. N. 1963 Kinematical hydromagnetic theory and its application to the low solar photosphere. *Astrophys. J.* **138**, 552–575.

PARKER, E. N. 1979 *Cosmical Magnetic Fields.* Clarendon.

PECKOVER, R. S. & WEISS, N. O. 1978 On the dynamic interaction between magnetic fields and convection. *Mon. Not. Roy. Astron. Soc.* **182**, 189–208.

PROCTOR, M. R. E. & GALLOWAY, D. J. 1978 The dynamic effect of flux ropes on Rayleigh–Bénard convection. *J. Fluid Mech.* **90**, 273–287.

PROCTOR, M. R. E. & WEISS, N. O. 1978 Magnetic flux ropes. In *Rotating Fluids in Geophysics* (ed. P. H. Roberts & A. M. Soward), pp. 389–408. Academic.

ROBERTS, P. H. 1967 *Introduction to Magnetohydrodynamics.* Longmans.

SPIEGEL, E. A. 1972 Convection in stars II. Special effects. *Ann. Rev. Astron. Astrophys.* **10**, 261–304.

THOMPSON, W. B. 1951 Thermal convection in a magnetic field. *Phil. Mag.* **42** (7), 1417–1432.

VERONIS, G. 1959 Cellular convection with finite amplitude in a rotating fluid. *J. Fluid Mech.* **5**, 401–435.

WALÉN, C. 1949 *On the Vibratory Rotation of the Sun.* Stockholm: Lindståhl.

WEISS, N. O. 1964 Convection in the presence of restraints. *Phil. Trans. Roy. Soc.* A **256**, 99–147.

WEISS, N. O. 1966 The expulsion of magnetic flux by eddies. *Proc. Roy. Soc.* A **293**, 310–328.

WEISS, N. O. 1975 Magnetic fields and convection. *Adv. Chem. Phys.* **32**, 101–107.

WEISS, N. O. 1977 Magnetic fields and convection. *Problems of Stellar Convection* (ed. E. A. Spiegel & J.-P. Zahn), pp. 176–187. Springer.